Modelling colloids with Baxter's adhesive hard sphere model

M A Miller† and D Frenkel‡

† University Chemical Laboratory, Lensfield Road, Cambridge CB2 1EW, U.K.
‡ FOM Institute for Atomic and Molecular Physics, Kruislaan 407, 1098 SJ Amsterdam, The Netherlands

E-mail: mam1000@cam.ac.uk, frenkel@amolf.nl

Abstract. The structure of the Baxter adhesive hard sphere fluid is examined using computer simulation. The radial distribution function (which exhibits unusual discontinuities due to the particle adhesion) and static structure factor are calculated with high accuracy over a range of conditions and compared with the predictions of Percus–Yevick theory. We comment on rigidity in percolating clusters and discuss the role of the model in the context of experiments on colloidal systems with short-range attractive forces.

1. Introduction

In contrast to atoms and small molecules, colloidal particles often interact through forces whose range is much shorter than the size of the particles themselves. The nature of such colloids and the origins of the forces are diverse, but the qualitatively similar form of the attraction leads to some common properties.

One of the most appealing systems of this type consists of hard spherical particles suspended in a solution of free polymer. An effective attraction of entropic origin arises between the spheres when they approach close enough to exclude the polymer from between them. This depletion effect can lead to colloidal phases analogous to all three of those expected in an atomic system: gas (low-density fluid), liquid (high-density fluid) and crystal [1]. The range and strength of the attraction can be varied continuously and independently by adjusting, respectively, the concentration and size of the polymer. The fully tunable character of the depletion interaction provides experiments with a flexibility that is not available in atomic systems and had previously been the privilege of theory and simulation [2]. Confocal microscopy further enables particle-by-particle determination of structure, providing wide scope for detailed interactions between experiment, theory and simulation.

Although there are firm theoretical foundations for adopting system-specific functional forms for the interaction potential between colloidal particles, such as that of Asakura and Oosawa [3] in the case of depletion, it is tempting to simplify the problem

as far as possible by retaining only the generic features of a hard repulsive core and short-range attractive tail. For this reason, colloidal systems are often modelled using a narrow square well potential. The phase diagram of the square well system is determined by the ratio of the well width to the hard core diameter, which is typically a few per cent in colloidal applications.

In 1968, Baxter introduced a model with a hard core and short-range attraction that is even simpler than the square well fluid in the sense that there is no range parameter [4]. Baxter considered the square well in a limit where the well depth, ϵ, becomes infinite while the well width, $d - \sigma$, becomes infinitesimal, σ being the hard core diameter and d the outer diameter of the well. The resulting potential, $U(r)$, is most easily defined by the corresponding Boltzmann factor as a function of the particle separation, r:

$$\exp[-U(r)/kT] = \Theta(r - \sigma) + \frac{\sigma}{12\tau}\delta(r - \sigma). \tag{1}$$

The first term in Equation (1) is a step function that forbids hard core overlap, while the second is a Dirac delta function that makes binary contacts energetically favourable to an extent determined by the parameter τ. Despite the apparently infinite strength of the attraction, the integrated weight of bound configurations of two adhesive hard spheres remains finite, and there is a thermodynamic equilibrium between bound and unbound states. Adhesion dominates at low τ, while ordinary hard spheres are recovered in the limit $\tau \to \infty$. We note that the thermal energy, kT, does not appear on the right-hand side of Eq. (1), but that τ may be regarded as an effective temperature. Indeed, Piazza *et al* found that the phase behaviour of lysozyme, electrostatically screened in a salt solution, is well described by the Baxter model if τ is taken to depend linearly on T [5]. A qualitatively different relationship can arise from other types of forces, and Mallamace *et al* found $\tau \propto 1/T$ for a micellar system [6]. In many colloidal systems, temperature is not the most relevant variable. In the case of depletion interactions, for example, the strength of the colloidal attraction is determined by the polymer concentration, and τ is a decreasing function of this variable [7].

These examples do not exhaust the wide variety of systems to which the Baxter model has been applied. Two other contrasting applications are emulsions of water droplets in oil [8] and 'hairy spheres' [9]. In the latter case, hard silica particles are grafted with short stearyl alcohol chains, and attraction between the spheres is induced when they are immersed in a solvent that is unfavourable for the chains, since aggregation excludes the solvent from between the particles.

A common device for mapping experimental results onto the Baxter model is to match the second virial coefficients. From Eq. (1) ones obtains $B_2 = B_2^{\mathrm{HS}}[1 - 1/(4\tau)]$, where $B_2^{\mathrm{HS}} = 2\pi\sigma/3$ is the hard sphere second virial coefficient. Having obtained τ, it is normal to interpret the experimental data by reference to the results of Percus–Yevick theory for the model. The phase diagram can be obtained through various routes of Percus–Yevick theory, the most commonly cited being the compressibility equation [4, 10], which predicts that the model undergoes a first-order phase transition between two fluid phases of different density. The energy equation also predicts such a transition

[11, 12], but the positions of the coexistence curve and the critical point are very different from the compressibility results.

A lack of definitive knowledge of the model's phase behaviour would clearly restrict its utility in the interpretation of experimental data. In recent work, we have used computer simulations to find numerical values for the critical point [13], coexistence curve, and equation-of-state [14] of adhesive hard spheres. We will refer to this work in the present contribution, but focus here on the structure of the fluid, providing high quality radial distribution functions and the corresponding static structure factors under a variety of conditions. The singular potential leads to unusual features in these functions.

2. Simulations

It is difficult to perform equilibrium simulations of systems with short range forces, since the energetically accessible fraction of configuration space decreases rapidly with narrowing of the attractive well. Exploring the relevant subspace ergodically by conventional molecular dynamics or Monte Carlo methods becomes a technical challenge.

The infinitesimal range of the Baxter potential has allowed a specialized approach to be devised for this model. Two particles only attract when they are precisely in contact, and the contact defines a spherical surface of radius σ if one of the particles is considered fixed and the remaining two degrees of freedom are explored. The total Boltzmann weight of the bound configuration can be found by integrating Eq. (1) over this surface. Because the spherical surface has zero thickness, it has no overlap with similar surfaces that describe contacts with other particles. Pursuing this property, it is possible to evaluate the weights of different bound states independently and then compare them. In contrast, the contact zone between two square-well particles is a spherical shell of finite thickness, and the overlap of such shells carves out increasingly complicated shapes as more shells become involved, making it difficult to find their volumes.

The possibility of comparing integrated Boltzmann weights has been exploited in a Monte Carlo algorithm dedicated to the adhesive hard sphere model, that moves particles by explicitly making and breaking contacts rather than by conventional random displacements [15, 16, 17]. Our own implementation is described in detail in Ref. [14]. Although the specialized algorithm is considerably more complicated than the standard Monte Carlo method, it can be used to sample ergodically in the limit of infinitesimal attractive range more efficiently than is possible using standard techniques on a potential of very narrow, but finite, range.

It is expected, however, that since the adhesive hard sphere model was originally derived from a square-well potential, the properties of the square-well fluid should approach those of Baxter's model as the range parameter, $\lambda = d/\sigma$, tends to unity. In Figure 1 we investigate this expectation for the case of the fluid–fluid critical point. The critical point in the Baxter limit was obtained numerically in previous work [13], while

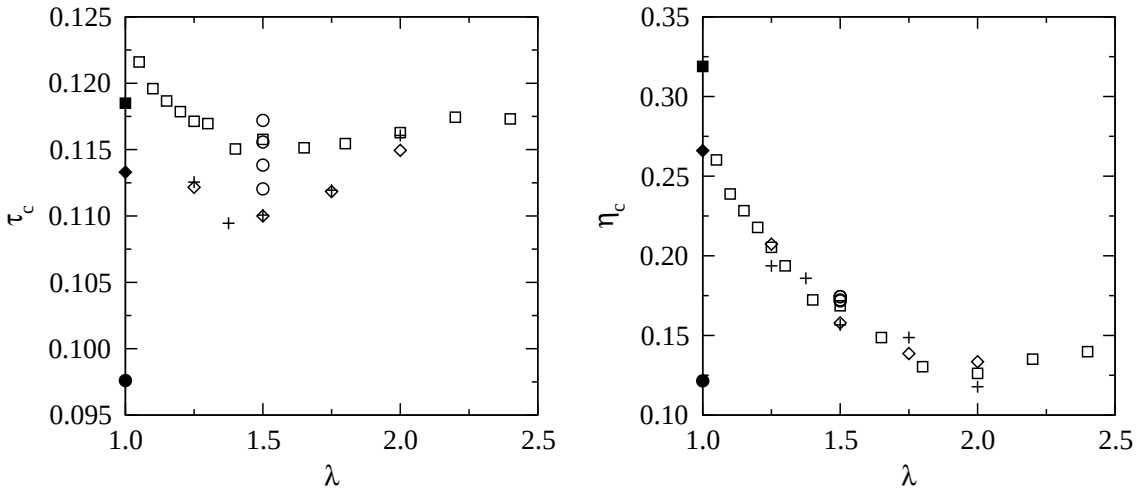

Figure 1. Critical effective temperature τ_c (left) and volume fraction η_c (right) of square-well fluids with range parameter λ. Open symbols are taken from References [18] (circles), [19] (squares), [20] (diamonds) and [21] (plusses). Filled symbols at $\lambda = 1$ are the adhesive hard sphere limits from the Percus–Yevick compressibility (circles) and energy (squares) routes, and from simulation (diamonds).

the square well data are taken from a number of simulation studies in the literature [18, 19, 20, 21]. In the right-hand panel of Figure 1, the square-well critical volume fractions extrapolate smoothly to the Baxter limit of 0.265 ± 0.005. Note that this value lies between the predictions of the compressibility and energy routes of Percus–Yevick theory [11], also marked in the Figure, and that these predictions differ by well over a factor of two.

To compare the critical temperatures, we need a method for mapping Baxter's τ parameter onto the thermodynamic temperature T of the square well. The most natural way to do this is probably through Baxter's expression $\epsilon/kT = -\ln[12\tau(1-\sigma/d)]$ that couples the square-well width and depth to define the adhesive limit [4]. Writing $\lambda = d/\sigma$ and rearranging, we obtain

$$\tau^{-1} = 12(1-\lambda^{-1})e^{\epsilon/kT}. \qquad (2)$$

The more general approach of equating the second virial coefficients yields a different expression that has the same form in the limit $\lambda \to 1$. The left-hand panel of Figure 1 shows that, under the mapping of Equation (2), there is remarkably little variation in the effective critical temperature τ_c with square-well range λ. Extrapolating the data of Lomakin *et al* [19] to $\lambda = 1$ in the left-hand panel of Figure 1 leads to a τ_c above the predictions of both routes of Percus–Yevick theory, as noted in Reference [19]. The more recent data of del Río *et al* lie systematically lower, and our simulation value [13] for the Baxter limit of $\tau_c = 0.1133 \pm 0.0005$ is somewhat below the Percus-Yevick energy result. We have observed that the simulated coexistence curve of the Baxter model suffers from strong finite-size effects near the critical point [13], and therefore employed a careful scaling analysis [22, 23, 24] to find the infinite-system τ_c. The apparent critical temperature of a finite system is generally an overestimate of the thermodynamic limit,

and if finite-size effects increase as the Baxter model is approached, they might account for the observed overshoot in some of the square-well data as $\lambda \to 1$. Backing off from the adhesive sphere limit, however, it is clear that the Percus–Yevick compressibility result of $\tau_c = 0.0976$—the value that is most often assumed—is a significant underestimate.

3. Structure of the adhesive hard sphere fluid

Figure 2 illustrates some instantaneous configurations from simulations of $N = 864$ particles at a fairly low volume fraction of $\eta = 0.164$. (The volume fraction is related to the number density $\rho = N/V$ by $\rho\sigma^3 = 6\eta/\pi$.) In the hard-sphere case, the particles fill the container uniformly. In the snapshot of adhesive hard spheres at $\tau = 0.13$, however, particles have aggregated into a number of clusters that are locally dense, leaving sizeable voids in the overall structure. A cluster is unambiguously defined as a set of particles connected by an unbroken chain of contacts. The largest cluster in the snapshot spans the simulation cell in the sense that it connects periodic images of the same particle once the periodic boundary conditions have been taken into account. Such a cluster is said to percolate and is the analogue of an infinite cluster in an experimental system. In some systems, the onset of percolation can be detected by a sudden change in a physical property, such as the electrical conductivity in a microemulsion [8]. If one defines a gel to be a non-compact space-filling structure of particles [25], then a system of adhesive hard spheres begins to exhibit gel-like properties when the volume fraction crosses the (τ-dependent) percolation threshold and infinite clusters are always present. However, it is important to remember that all clusters are dynamic, since particles are not irreversibly bound. Indeed, the conditions of Figure 2(b) lie on the percolation threshold itself [14], where the lifetime of a percolating cluster is very short and may be determined by the removal of a single particle.

The effect of surface adhesion on the structure of the fluid is more clearly seen in the radial distribution function, $g(r)$, which is shown in Figure 3 for the same conditions as the snapshots in Figure 2. At this low volume fraction, the hard sphere fluid (dotted line) shows little structure. In contrast, the adhesive hard sphere fluid has a number of striking features. Physical clusters in which the separation of two particles cannot be changed without breaking a contact contribute a delta-function to $g(r)$, since a single geometry then receives a finite statistical weight. The delta-functions appear to have finite height in Figure 3 due to the finite bin width (0.002σ) used in accumulating $g(r)$. The smallest clusters that make delta-function contributions at distinct distances contain 2, 5 and 6 particles, as illustrated in Figure 3. The darker particles indicate the separations corresponding to the peaks, which are located at $r/\sigma = 2$, $\sqrt{8/3}$ and $5/3$. The tendency for particles to bind, which gives rise to the strong delta-function at $r = \sigma$, also explains the contrasting trend in $g(r)$ from ordinary hard spheres in the range $1 < r/\sigma < 2$: the presence of a tightly-bound shell of nearest neighbours excludes other particles from this range, resulting in a deficit of particles close to $r = \sigma$ relative to the bulk density. The surplus exhibited by hard spheres indicates a more loosely

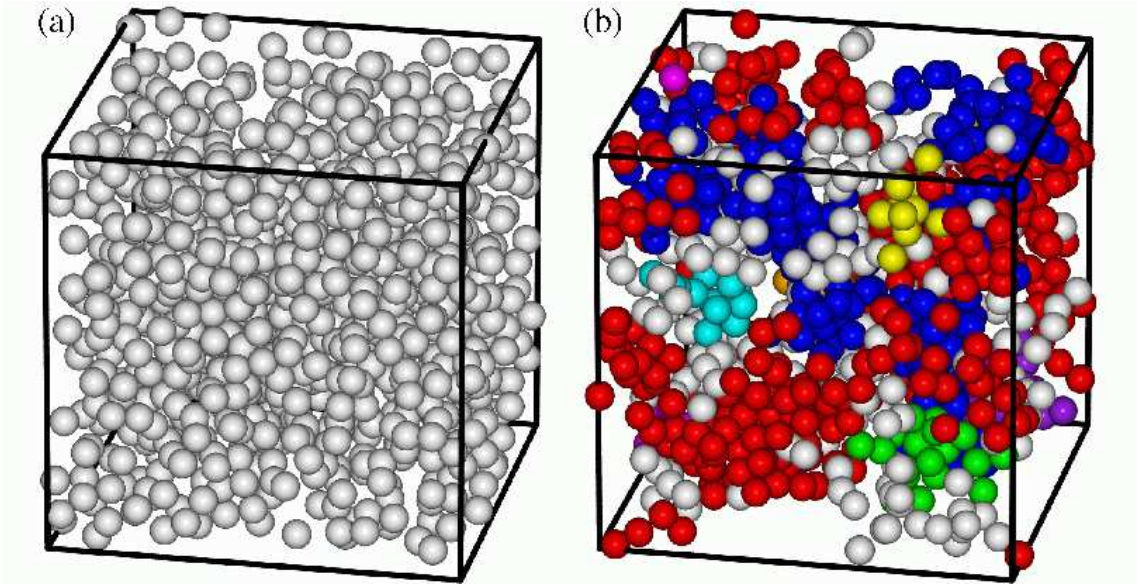

Figure 2. Simulation snapshots of $N = 864$ particles at a volume fraction of $\eta = 0.164$. Left: ordinary hard spheres, right: adhesive hard spheres at $\tau = 0.13$. The largest clusters have been highlighted in colour. The red cluster percolates.

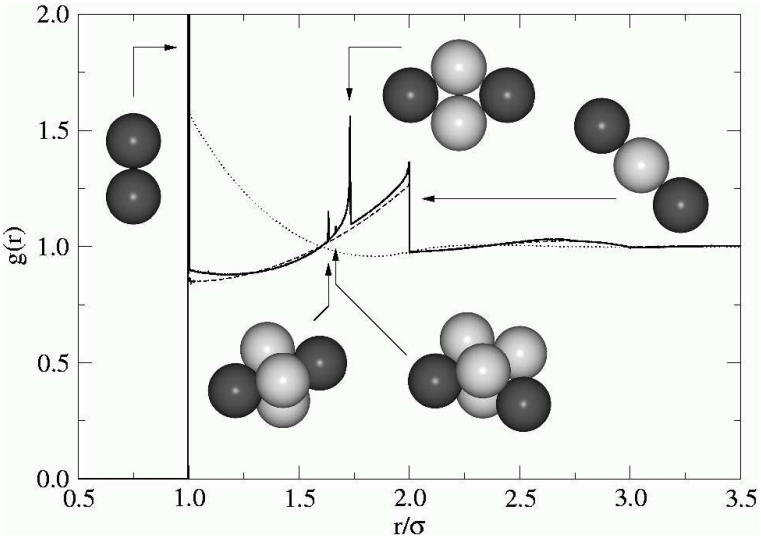

Figure 3. Radial distribution function, $g(r)$, at a volume fraction of $\eta = 0.164$ as for Figure 2. Solid line: adhesive hard spheres at $\tau = 0.13$ from simulation; dashed line: the corresponding Percus–Yevick prediction; dotted line: hard spheres. Physical clusters contributing to certain features of the solid line are indicated.

structured coordination shell arising purely from excluded volume considerations.

In addition to the singularities, $g(r)$ has two discontinuities in the range plotted in Figure 3. Discontinuities arise when the distance between two particles in a flexible cluster is extremized with respect to variation of the cluster geometry while the topology of contacts is held fixed. Consider, for example, the trimer illustrated in Figure 3. Without breaking or making any contacts (and therefore without changing the energy),

the cluster can be continuously deformed between an equilateral triangle, where the dark particles are separated by σ, to the linear structure shown, where the separation is 2σ. A greater separation would require the breaking of a bond. Similarly, the tetramer can be deformed continuously to give separations between σ and $\sqrt{3}$ without altering the topology of contacts.

Cummings *et al* have noted that, within the framework of Percus–Yevick theory for this model, a discontinuity in the n^{th} derivative of the radial distribution function at r gives rise to a discontinuity in the $(n+1)^{\text{th}}$ derivative at $r+\sigma$ [26]. Hence, the delta-function at $r=\sigma$ gives rise to the discontinuity at $r=2\sigma$, which in turn causes the discontinuous gradient at $r=3\sigma$, also reproduced by the simulations. Percus–Yevick theory, however, neglects certain cluster diagrams, causing it to miss many of the other delta-functions and discontinuities accounted for in the simulations. Glandt and coworkers have provided expressions for many low-order cluster integrals, and used them to calculate cluster concentrations and delta-function coefficients for $g(r)$ [27, 16].

We are now in a position to calculate structural properties of the adhesive hard sphere fluid more precisely than was previously possible [17]. In Figure 4 we present the radial distribution function and the static structure factor, $S(q)$, for a series of conditions considered by Kranendonk and Frenkel [17], although we omit the combination $\tau=0.1$, $\eta=0.14$ as this lies within the spinodal region of the phase diagram. $S(q)$ is related to $g(r)$ by a Fourier transform, but is calculated in the simulations directly from $S(q)=\langle\rho(\mathbf{q})\rho(-\mathbf{q})\rangle$, where

$$\rho(\mathbf{q})=\sum_{i}^{N}\exp(-\mathbf{q}.\mathbf{r}_i) \tag{3}$$

and $\mathbf{r}_i$ is the position of particle i. Because of the periodic boundary conditions, it is only possible to study fluctuations with $\mathbf{q}=2\pi L^{-1}(q_x,q_y,q_z)$ where q_x, q_y, and q_z are all integers and L is the length of the cubic simulation cell. 2000 $\mathbf{q}$-vectors with randomly-chosen orientation were sampled, covering the range plotted approximately uniformly.

Notwithstanding the failure of Percus–Yevick theory to capture all but one of the delta-functions labelled in Figure 3, the agreement between theory and simulation is good, and improves as τ increases, corresponding to less dominant surface adhesion. The delta-functions, however, are a defining feature of the adhesive hard sphere model, and the omission of the corresponding cluster integrals is presumably one of the reasons for the significant difference between the equations of state derived through different functionals from the Percus–Yevick $g(r)$.

The theory does remarkably well for the prefactor of the delta-function at $g(\sigma)$, which is directly proportional to the average coordination number (number of contacts per particle). The Percus–Yevick coordination number is available in simple closed form [28] and under the three sets of conditions displayed in Figure 4 takes the values 2.93, 2.51 and 2.65 respectively, to be compared with 2.97, 2.48 and 2.69 from simulation (the latter being converged to within the precision quoted). For a very recent analysis

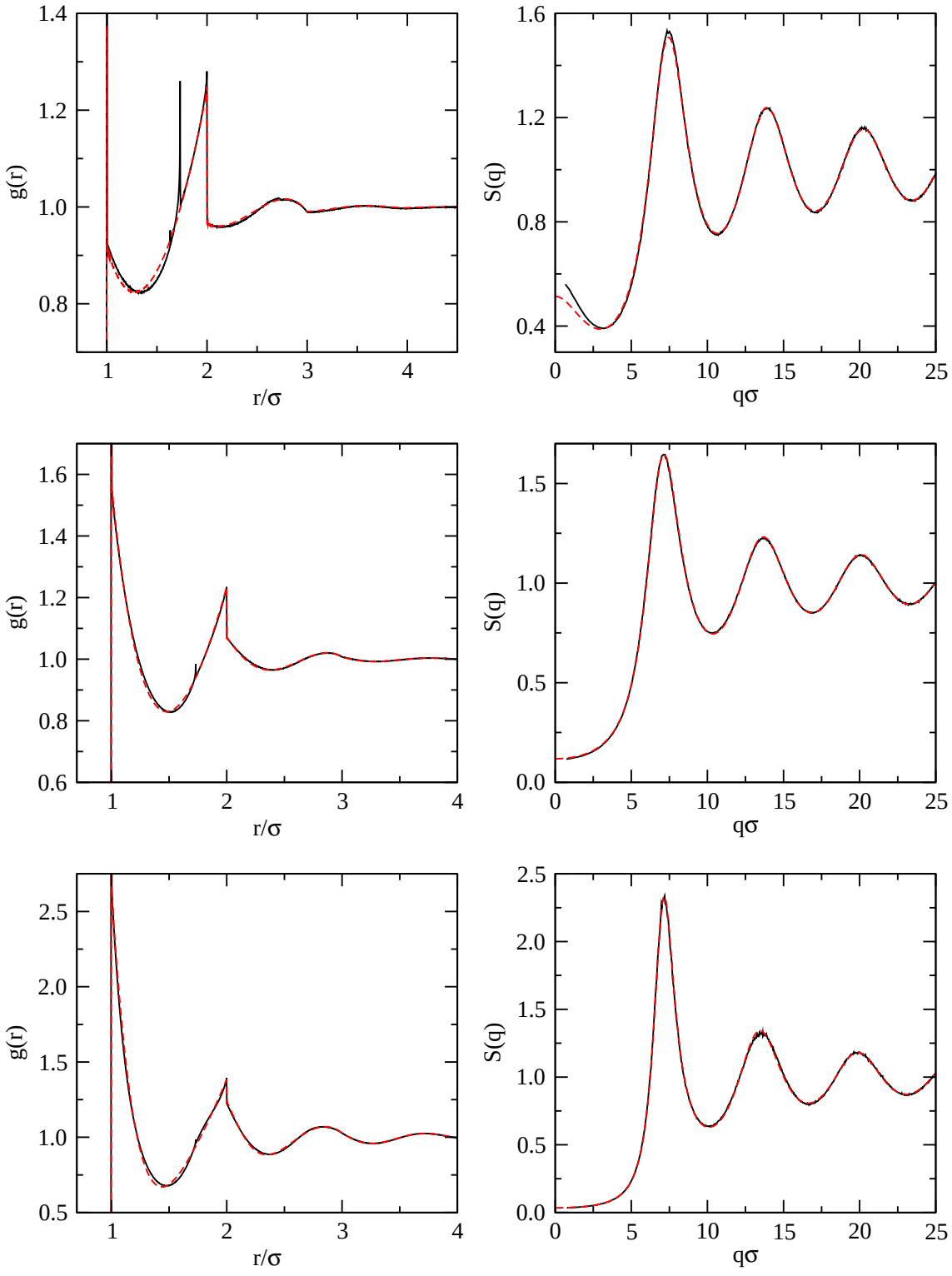

Figure 4. Radial distribution function (left) and static structure factor (right) under three sets of conditions: $\tau = 0.2$, $\eta = 0.32$ (top row); $\tau = 0.5$, $\eta = 0.4$ (middle row); $\tau = 1$, $\eta = 0.5$ (bottom row). Solid black lines are from simulation and dashed red lines from Percus–Yevick theory.

of adhesive hard spheres in the theoretical framework of a generalized closure that subsumes the Percus–Yevick see Reference [29], which includes comparisons with the data in Figure 4.

4. Rigidity

The percolation threshold denotes the set of conditions on the phase diagram at which the cluster size diverges, or in a simulation, at which system-spanning clusters are observed with a probability of 50%. (The transition to percolation is sharp, and the 50% criterion, though arbitrary, is robust.) As the threshold is crossed, thermodynamic properties and their derivatives change smoothly, and so percolation is not a thermodynamic phase transition. The connectivity of the particles may, however, lead to sudden changes in other properties such as electrical conductivity [8].

A percolating cluster is defined only by its connectivity through the system. In principle, a connected cluster with only a minimum of connections can be deformed without making or breaking any contacts between particles and therefore without any energetic penalty. In contrast to this 'bond percolation' one might expect a change in mechanical properties if a percolating cluster contained a rigid backbone that, due to its network of contacts, cannot be deformed without altering its topology. To find whether a cluster exhibits such 'rigidity percolation' one must discount any 'floppy' (non-rigid) modes, and determine whether the structure remains constrained [30]. Because of the additional contacts required to constrain the geometry, any rigidity percolation threshold is expected to lie to the high-density side of the bond percolation threshold on the phase diagram.

In a system of adhesive hard spheres, the smallest rigid subunit is a maximally connected tetrahedron, which possesses six contacts. Larger rigid structures can be produced by adding triply-coordinated particles to the faces of the tetrahedron, producing a network of face-sharing tetrahedra. Two tetrahedra may be connected by a common edge or vertex, but such connections lend flexibility to the overall cluster. We may therefore determine the extent of rigidity by searching for face-sharing polytetrahedral networks.

Figure 5 illustrates some snapshots from a rigidity analysis of adhesive hard spheres at $\tau = 0.13$ and two volume fractions, both of which lie within the bond-percolated regime. As the left-hand panels show, most particles belong to the bond-percolating cluster. In the right-hand panels, the rigid subunits are displayed in different colours, and particles possessing independent unconstrained degrees of freedom are not shown. It is clear that, even at a high volume fraction of $\eta = 0.50$, rigidity does not extend further than a few particles. Several rigid tetrahedra share one or two particles (in which case the assignment of the shared particles to either tetrahedron is arbitrary), but it is rare to see a fully constrained unit of more than six particles.

As the volume fraction of the system approaches its maximum, the physical space available to floppy modes tends to zero, and mechanical properties should change

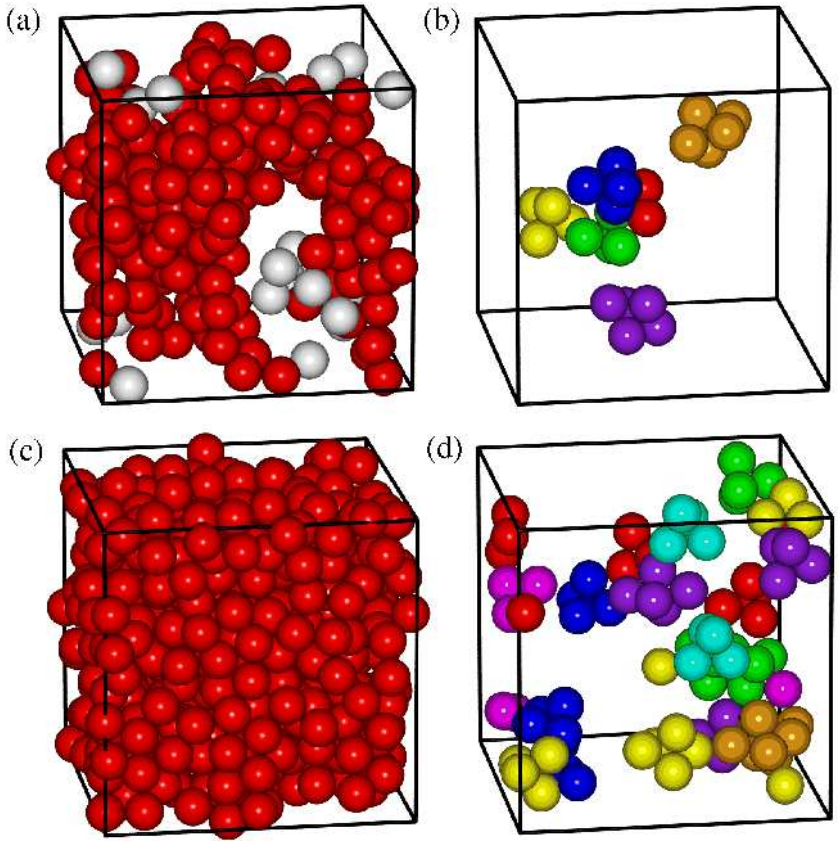

Figure 5. Snapshots from grand canonical simulations [14] at $\tau = 0.13$. All particles are shown in the left-hand frames, with particles in the percolating cluster coloured red. On the right, any particles not belonging to a rigid subunit have been removed, and different colours are used to distinguish between the subunits. Frames (a) and (b) are taken from simulations with an average packing fraction of 0.17, and (c) and (d) an average of 0.50.

accordingly. However, as we find no evidence for a rigidity percolation threshold in this system, we expect these changes to occur smoothly rather than showing any sharp transitions.

5. Some remarks: gels and glasses

Finally, we comment on the adhesive sphere fluid in the context of recent work on glasses. Mode-coupling theory for particles with sufficiently short-range attractive forces predicts two types of structural arrest: a 'repulsive' glass in which particles are trapped within the local cage of their neighbours at high volume fraction, and an 'attractive glass' where particles are energetically bound to their neighbours even at lower volume fraction. There is a re-entrant glass–liquid–glass transition as a function of adhesive strength at constant volume fraction and a line of glass–glass transitions extending from the point where the two liquid–glass lines meet [31]. These predictions are borne out in experiments [32] and simulations [33].

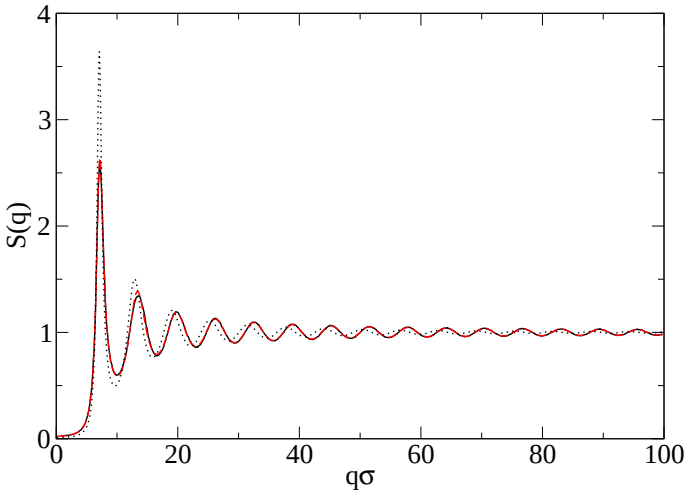

Figure 6. Static structure factor of adhesive hard spheres at $\tau = 1.32$ and $\eta = 0.52$, illustrating its slowly-decaying $1/q$ tail. The solid black line is from simulation and the dashed red line from Percus–Yevick theory. For comparison, the dotted line shows the simulation result for ordinary hard spheres at the same volume fraction.

Being the archetypal short-range attractive system, it seems natural to apply the mode-coupling analysis to the Baxter model. There are, however, at least two obstacles to doing this directly. From the simulation approach, Monte Carlo techniques allow us to probe the thermodynamics and equilibrium structure of adhesive hard spheres, but do not provide rigorous information on dynamic processes. Since the time-scales for bond making and breaking diverge as the adhesive limit is approached [34], direct molecular dynamics simulations are not feasible. From the point of view of mode-coupling theory, the Baxter limit is problematic because the structure factor, which is the main input to the theory, contains a slowly decaying $(1/q)$ tail that makes the integral over q in the mode-coupling functional diverge. It is therefore necessary to introduce an arbitrary reciprocal-space cutoff $q_{\max}$ upon which the results depend [31, 35].

Considering the static structure factor as the Fourier transform of the radial distribution function, the $1/q$ term in $S(q)$ arises specifically from the delta-function at $r = \sigma$ in $g(r)$. The slowly-decaying tail is well reproduced by simulation, as illustrated in Figure 6 for $\tau = 1.32$, $\eta = 0.52$. These conditions are close to the region of the phase diagram where the attractive and repulsive glass lines meet [31]. The plot also serves to demonstrate that Percus–Yevick theory works well for $S(q)$ in the regime of greatest relevance to mode-coupling theory.

Figure 7 shows the phase diagram of adhesive hard spheres with the fluid–fluid coexistence line and (bond) percolation threshold as determined by simulation [14]. Infinite clusters dominate the system to the high-η side of the percolation threshold. The threshold demarks the well-defined set of conditions where the structure of the fluid first becomes connected on a macroscopic scale and (due to its low overall volume fraction) locally inhomogeneous in density, unlike a normal liquid. On structural grounds, therefore, we may think of the percolated part of the phase diagram as a gel,

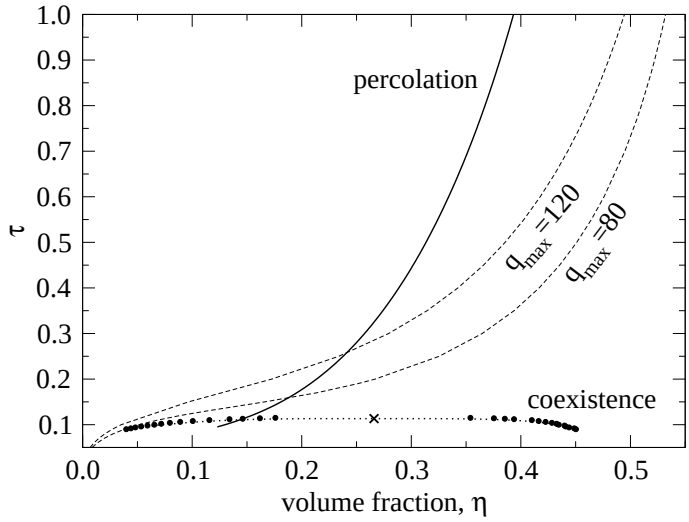

Figure 7. Phase diagram of adhesive spheres in the η–τ plane. The dotted line with circles is the fluid–fluid coexistence curve from simulation, with the critical point marked by a cross [13]. The solid line is the percolation threshold from simulation [14] to the high-η side of which infinite clusters exist in the system. The dashed lines are the mode-coupling attractive glass transition with cutoffs $\sigma q_{\max} = 80$ and 120 as marked. Mode-coupling theory predicts structural arrest to the high-η side of this threshold.

even though crossing the percolation threshold itself is not accompanied by immediate structural arrest. Progressing further into the percolated regime, the infinite clusters become bolstered with more neighbours. It then requires many bonds to be broken simulataneously for a given cluster to stop percolating, and the connectedness of the cluster becomes far less transitory.

For comparison, Figure 7 also shows two lines corresponding to the attractive glass transition from mode-coupling theory [31] with two values of the cutoff $q_{\max}$. The range of the τ axis extends to somewhat below the meeting point of the attractive and repulsive glass transitions, and the latter therefore does not appear on this plot. To the high-η side of the attractive glass line, mode-coupling theory predicts the fluid to by structurally arrested due to the dominance of adhesion between particles. Although the lines are shown all the way down to low volume fraction, mode-coupling theory is expected to be most reliable at high volume fraction, where the equilibrium structure factor is likely to resemble that of the arrested phase quite closely. In contrast, it is questionable whether the equilibrium $S(q)$ can be used to predict structural arrest—by definition a non-equilibrium property—at densities low enough for the structure to differ significantly from equilibrium. Indeed, at very low volume fraction, the average number of bonds per particle is not sufficient to support large clusters at all [36].

The two dashed curves in Figure 7 illustrate the effect of increasing $q_{\max}$ in mode-coupling theory, which is to assign more of the phase diagram to the attractive glass state. Towards the high volume-fraction ends of these lines (where they are expected to be most reliable), they approximately parallel the percolation threshold. The physical

interpretation of introducing a q-space cutoff is to back off from the limit of infinitesimal attractive range. The square-well ranges corresponding to $\sigma q_{\max} = 80$ and 120 may be estimated to be about $\lambda = 1.04$ and 1.026, respectively [37]; both are relevant for experimental applications in colloids. While the attractive-glass line should in principle continue to advance indefinitely to lower densities as $q_{\max}$ is increased, it probably makes little sense to consider anything to the low-η side of the percolation threshold as glassy, since in that regime the system is a fluid of separated and fluctional clusters. Therefore, while the percolation threshold does not contain dynamical information, it nevertheless retains an important utility as an unambiguous transition to a system-wide connected state which, as we have argued, possesses at least some properties of a gel.

It is also apparent from Figure 7 that the critical point for the fluid–fluid separation of adhesive hard spheres lies both within the percolated part of the phase diagram and inside the attractive glass region even for q-space cutoffs somewhat smaller than $80/\sigma$ (and corresponding ranges longer than $\lambda = 1.04$). The assertion made in previous work [13], that gelation is likely to interfere with equilibrium phase separation in systems with short-range attractive forces, therefore remains highly plausible.

Acknowledgments

MAM is very grateful to Dr. Matthias Sperl for the MCT data plotted in Figure 7 and for discussions regarding the application of MCT to the Baxter model. The work of the FOM Institute is part of the research program of FOM and is made possible by financial support from the Netherlands Organization for Scientific Research (NWO).

References

[1] S. M. Ilett, A. Orrock, W. C. K. Poon and P. N. Pusey, Phys. Rev. E **51**, 1344 (1995).
[2] D. Frenkel, Science **296**, 65 (2002).
[3] S. Asakura and F. Oosawa, J. Chem. Phys. **22**, 1255 (1954).
[4] R. J. Baxter, J. Chem. Phys. **49**, 2770 (1968).
[5] R. Piazza, V. Peyre and V. Degiorgio, Phys. Rev. E **58**, R2733 (1998).
[6] F. Mallamace, P. Gambadauro, N. Micali, P. Tartaglia, C. Liao and S.-H. Chen, Phys. Rev. Lett. **84**, 5431 (2000).
[7] S. Ramakrishnan, M. Fuchs, K. S. Schweizer and C. F. Zukoski, J. Chem. Phys. **116**, 2201 (2002).
[8] S. H. Chen, J. Rouch, F. Sciortino and P. Tartaglia, J. Phys. Cond. Mat. **6**, 10855 (1994).
[9] H. Verduin and J. K. G. Dhont, J. Colloid Interface Sci. **172**, 425 (1995).
[10] B. Barboy, J. Chem. Phys. **61**, 3194 (1974).
[11] R. O. Watts, D. Henderson and R. J. Baxter, Adv. Chem. Phys. **21**, 421 (1971).
[12] B. Barboy and R. Tenne, Chem. Phys. **38**, 369 (1979).
[13] M. A. Miller and D. Frenkel, Phys. Rev. Lett. **90**, 135702 (2003).
[14] M. A. Miller and D. Frenkel, submitted (2004).
[15] N. A. Seaton and E. D. Glandt, J. Chem. Phys. **84**, 4595 (1986).
[16] N. A. Seaton and E. D. Glandt, J. Chem. Phys. **87**, 1785 (1987).
[17] W. G. T. Kranendonk and D. Frenkel, Mol. Phys. **64**, 403 (1988).
[18] N. V. Brilliantov and J. P. Valleau, J. Chem. Phys. **108**, 1115 (1998).
[19] A. Lomakin, N. Asherie and G. B. Benedek, J. Chem. Phys. **104**, 1646 (1996).

[20] F. del Río, E. Ávalos, R. Espíndola, L. F. Rull, G. Jackson and S. Lago, Mol. Phys. **100**, 2531 (2002).
[21] L. Vega, E. de Miguel, L. F. Rull, G. Jackson and I. A. McLure, J. Chem. Phys. **96**, 2296 (1992).
[22] A. D. Bruce and N. B. Wilding, Phys. Rev. Lett. **68**, 193 (1992).
[23] N. B. Wilding and A. D. Bruce, J. Phys. Cond. Mat. **4**, 3087 (1992).
[24] N. B. Wilding, Phys. Rev. E **52**, 602 (1995).
[25] W. C. K. Poon and M. D. Haw, Adv. Colloid Interface Sci. **73**, 71 (1997).
[26] P. T. Cummings, J. W. Perram and E. R. Smith, Mol. Phys. **31**, 535 (1976).
[27] A. J. Post and E. D. Glandt, J. Chem. Phys. **84**, 4585 (1986).
[28] Y. C. Chiew and E. D. Glandt, J. Phys. A **16**, 2599 (1983).
[29] D. Gazzillo and A. Giacometti, J. Chem. Phys. **120**, 4742 (2004).
[30] D. J. Jacobs and M. F. Thorpe, Phys. Rev. Lett. **75**, 4051 (1995).
[31] K. Dawson, G. Foffi, W. Götze, F. Sciortino, M. Sperl, P. Tartaglia, T. Voigtmann and E. Zaccarelli, Phys. Rev. E **63**, 011401 (2001).
[32] K. N. Pham, A. M. Puertas, J. Bergenholtz, S. U. Egelhaaf, A. Moussaïd, P. N. Pusey, A. B. Schofield, M. E. Cates, M. Fuchs and W. C. K. Poon, Science **296**, 104 (2002).
[33] A. M. Puertas, M. Fuchs and M. E. Cates, Phys. Rev. Lett. **88**, 098301 (2002).
[34] G. Stell, J. Stat. Phys. **63**, 1203 (1991).
[35] L. Fabbian, W. Götze, F. Sciortino, P. Tartaglia and F. Thiery, Phys. Rev. E **59**, R1347 (1999).
[36] E. Zaccarelli, G. Foffi, K. A. Dawson, F. Sciortino and P. Tartaglia, Phys. Rev. E **63**, 031501 (2001).
[37] W. Götze and M. Sperl, J. Phys. Cond. Mat. **15**, S869 (2003).